www.czasopisma.pan.pl PAN POLSKA AKADEMIA NAUK www.journals.pan.pl

Arch. Metall. Mater. **65** (2020), 3, 1217-1221

DOI: 10.24425/amm.2020.133241

M. MOSIAŁEK[1*], M. ZIMOWSKA[1], D. KHARITONOV[1], M. GÓRSKI[1],
M. KRZAN[1], A. KOMENDA[2]

DUAL PORE CATHODE MATERIALS FOR SOLID OXIDE FUEL CELLS

In this work, we developed the lanthanum strontium cobalt ferrite and it's composite with yttrium iron cobaltite (mass ratio of 1:1) cathodes as a thin layer on $Ce_{0.8}Sm_{0.2}O_{1.9}$ electrolyte. Two kinds of electrode pastes were prepared, with and without 6 mm polystyrene beads as an additional pore former. The performance of cathode materials was investigated by electrochemical impedance spectroscopy as a function of electrode morphology, oxygen partial pressure, potential, and temperature. The polarization resistance of the more porous electrodes was lower than those electrodes prepared without additional pore former in the whole potential range at 800°C, slightly lower at 700°C and 600°C. The addition of yttrium iron cobaltite decreased the performance of both types of cathodes. The lower polarization resistance of porous cathodes is due to the facilitated gas diffusion through their structure.

Keywords: solid oxide fuel cell, yttrium iron cobaltite, lanthanum strontium cobalt ferrite, composite cathode, electrochemical impedance spectroscopy

1. Introduction

Solid oxide fuel cells (SOFC) as the power generators have the theoretical conversion efficiency of the stored in fuel chemical energy into electrical energy close to 100% [1] and highest among all types of fuel cells [2]. Recently, efforts have been devoted to the development of SOFC working in lower and lower temperatures. The slow oxygen reduction reaction on a cathode is the main source of energy losses. Now, the research community is focused on the development of new effective cathode materials working in the intermediate temperature range (IT) (500-800°C) and low-temperature range (350-500°C). Lanthanum strontium cobalt ferrite (LSCF) is the state-of-the-art cathode material for the IT range. LSCF exhibits excellent catalytic activity in oxygen reduction reaction (ORR), ionic conductivity (greater than 215 S cm^{-1} at 550°C) [3] and electronic conductivity [4]. Composite cathodes containing a second active component in addition to LSCF may exhibit better properties than pure LSCF cathodes. The addition of the electrolyte material to the cathode material is the most popular practice [5]. It allows to improve the ionic conductivity and reduce the high thermal expansion coefficient (TEC). The catalytic activity [6-8] can be improved by the addition of noble metals [6-8] or due to the addition of another cathode material (even less active than LSCF) [9-12].

Recently reported $YFe_{0.5}Co_{0.5}O_3$ (YFC) cathode material reveals very low polarization resistance (R_p) of 0.07 W cm^2 at 750°C. Moreover, it has not too large TEC equal to 15-20 × 10^{-6} K^{-1} in the IT range and excellent conductivity 183 S cm^{-1} at 750°C [13]. YFC seems to be an excellent candidate for the second phase in the composite cathode for SOFCs.

Another issue limiting the performance of the cathode is its microstructure. LSCF is an excellent mixed ionic-electronic conductor. ORR occurs at the interface cathode/gas phase [14]. The surface area of that interface rises with increasing porosity and the thickness of the cathode, which may lead to a decrease in the R_p [15,16]. Although in thicker cathodes gas diffusion resistance, as well as electronic and ionic resistances, restrict the decrease of R_p. It was shown that the addition of the organic polymer beads to the lanthanum strontium manganite cathode paste leads to the dual pore structure of the sintered cathode which facilitates its infiltration by silver nitrate solution for the introduction of silver as the second phase [17].

In the present work, we checked if the performance of the LSCF cathode can be improved due to the addition to the LSCF cathode ink either YFC and/or 6 mm polystyrene beads, causing dual pore size structure.

[1] JERZY HABER INSTITUTE OF CATALYSIS AND SURFACE CHEMISTRY, POLISH ACADEMY OF SCIENCES, NIEZAPOMINAJEK 8, PL-30239 KRAKOW, POLAND
[2] RESEARCH AND DEVELOPMENT CENTER OF TECHNOLOGY FOR INDUSTRY, 59 ZŁOTA STR., 00-120 WARSZAWA, POLAND

* Corresponding author: nbmosial@cyfronet.pl

2. Experimental

2.1. Materials

$Ce_{0.8}Sm_{0.2}O_{1.9}$ electrolyte disks were elaborated from commercial powder (Terio Inc., Qingdao, China) and sintered for 2 h at 1500°C as described in [18]. Y_2O_3 (Onyxmet) dissolved in nitric acid was added to the solution of iron and cobalt nitrates (both Sigma Aldrich, reagent grade) in stoichiometric proportions, then citric acid (Sigma Aldrich, reagent grade) was added and the solution was dried and obtained gel was calcined at 950°C for 10 h. The $YFe_{0.5}Co_{0.5}O_3$ cathodic powder of perovskite structure [19] was obtained as is described in [17]. The LSCF and organic vehicle (all Nexceris) were used for the preparation of cathode pastes. Polystyrene balls of 6 μm in diameter (Micro Beads) were added to the inks for creating of grater pores in the part of sintered electrodes. Such electrodes are denoted in this work with the suffix –PS.

The electrolyte disks of 20 mm diameter were cut in half. The cathode pastes containing ink vehicle, and following cathode materials LSCF, LSCF and YFC (1:1), LSCF and polystyrene balls as well as LSCF, YFC and polystyrene balls, were applied on the surface of the electrolyte half-disk. The Matte Finish Magic Tape (Scotch) of 0.15 mm thickness was used as a shaping mask forming two identical round working and reference electrodes (Fig. 2c in [18]), whereas on the whole rear side of the electrolyte disk the LSCF counter electrode was screen printed. The samples were sintered for 2 h at 1000°C with heating and cooling rates 1°C min^{-1}. Obtained cells were mounted in the alumina text fixture detailed sketched in [20].

2.2. Methods

The structure of the powder was checked with the X'Pert PRO (PANalytical B.V.) diffractometer operated at 40 kV and 30 mA by using Ni-filtered Cu Kα radiation.

The morphology of the samples was carried out by means of JEOL JSM-7500F field emission scanning electron microscope equipped with the energy dispersive X-ray spectroscopy (EDS) INCA PentaFetx3 EDS detection system of characteristic X-ray radiation.

Electrochemical measurements were performed using 300 series potentiostat/galvanostat/ZRA in the three-electrode setup in oxygen (99.5%, Air Liquide Polska) and the mixture of oxygen and argon (99.999%, Air Liquide Polska) in defined proportions. The electrochemical impedance spectroscopy (EIS) spectra were recorded in the 10 mHz-300 kHz frequency range with a density of 8 frequency points per decade. The sinusoidal voltage of the amplitude 5 mV rms was applied. EIS parameters were calculated by fitting the impedance equation proper for the assumed equivalent electrical circuit (EEC) to the obtained data. The data-treatment procedure and the quality of the fit were characterized by the standard deviation as is described in previous work [21].

3. Results and discussion

The microstructure of YFC sintered powder and prepared cells are presented in Fig. 1. The obtained cathodes were 60-80 μm thick. The 6 μm in diameter holes were evenly distributed in cathodes prepared with polystyrene balls.

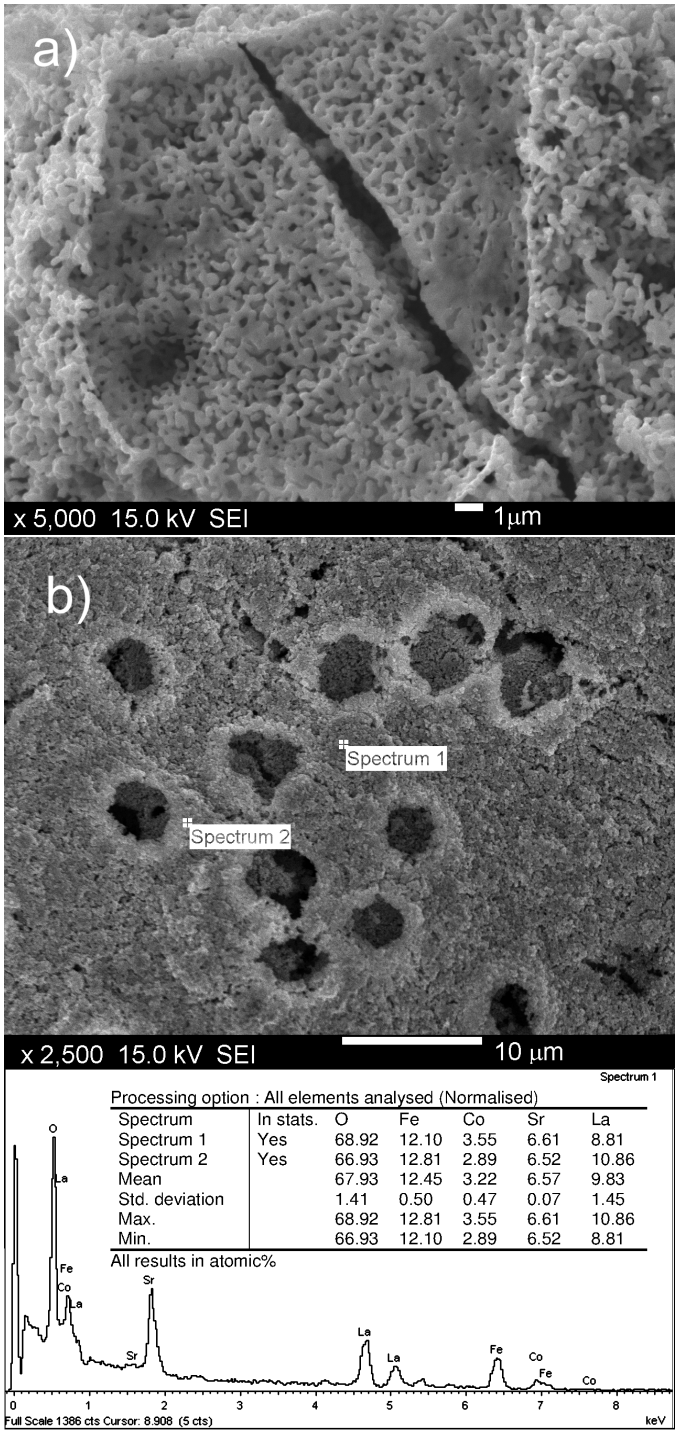

Fig. 1. SEM images of (a) YFC powder; (b) the LSCF-PS electrode surface with EDX analysis

The impedance spectra recorded at 800°C contain an inductive loop and three strongly overlapped capacitive semicircles (Fig. 2). The spectra recorded at 700 and 600°C contain one

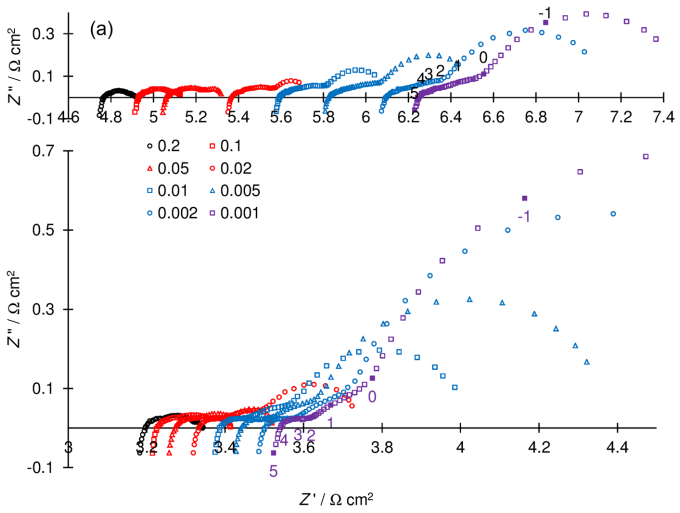

Fig. 2. Examples of EIS spectra of LSCF (a) and LSCF-PS (b) electrodes in Nyquist representation at 800°C in oxygen and mixtures of argon and oxygen; $P(O_2)\ P^{-1}$ in the legend; the numbers near filled experimental points denote the logarithm of the frequency

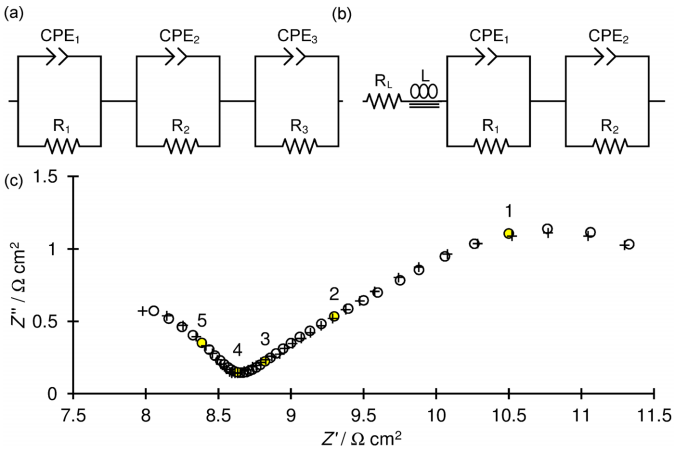

Fig. 3. Equivalent electrical circuits used to fit the data (a) and (b); example of the fit, LSCF-YFC-PS electrode, 700°C, $P(O_2)\ P^{-1} = 0.1$, crosses – measured data, circles – fitted data; the numbers above filled points denote the logarithm of the frequency (c)

separated high-frequency semicircle, which can be ascribed to the electrolyte grain boundary process and two or three overlapped capacitive semicircles, which can be ascribed to the electrode processes. The assumed EECs contain 2 or 3 connected in series sub-circuits, each contains resistance and capacitance parallel connected (R, C) and an inductance for spectra recorded at 800°C or additional (R, C) sub-circuit for spectra recorded at lower temperatures.

Each capacitor is replaced by the constant phase element (CPE).

The impedance of the CPE can be expressed by the following formula [21]:

$$Z_{CPE_i} = \frac{1}{2\pi f_0 C_i}\left(\frac{f_0}{jf}\right)^{\alpha} \tag{1}$$

where: f is the frequency, f_0 is the frequency of reference assumed $f_0 = 1$ kHz [21], C_i is the capacitance at the frequency of reference, j is an imaginary unit, index i is the number of (R, CPE) pairs, and α is a coefficient, which value should be in the range from 0.5 to 1 (usually, its values are in the range of 0.8-1.0, while for diffusion processes α is close to 0.5). The polarization resistance (R_p) was calculated as the sum of all resistances representing electrode processes. The EECs used and an example of the fit are presented in Fig. 3.

The polarization resistance of LSCF and LSCF-PS electrodes versus applied potential are compared in Fig. 4. LSCF-PS electrode reveals much smaller R_p in the whole potential range at 800°C, slightly smaller at 700°C and 600°C. It is worth noting that if the cathode is polarized with negative potential, a direct current proportional to the applied potential flows through it. The cathodic reaction:

$$O_2 + 4e^- \rightarrow 2O^{2-} \tag{2}$$

consumes gaseous oxygen lowering its concentration in the surrounding gas. The fastest gas exchange takes place in the cathode layer which is located directly under the flow of gas feeding the cell, while in the deeper layers closer to the electrolyte the gas exchange is slower and, therefore, the gas atmosphere is poorer in oxygen due to the reaction (2). The decrease in oxygen concentration in the deeper layers of the cathode is greater at the more cathodic applied potentials. The dependences shown in Fig. 4 reveal that the difference in polarization resistance of both types of electrodes at 800°C is increasing with increasing negative potential, whereas at 700 and 600°C this difference is negligible for the small negative polarization and significant for a more negatively polarized electrode. Adler et al. [14] showed that for an LSCF electrode at 700°C below a certain concentration of oxygen, an additional relatively large capacitive semicircle appears in the impedance spectrum, in other words, there is a sharp increase in polarizing resistance. A similar dependence of polarization resistance on oxygen concentration was reported by Murray et al. [22]. These authors showed that the polarization resistance of the LSCF electrode increases slowly with a decrease in oxygen concentration, whereas below $P(O_2) = 0.02$ it increases very fast [22]. The observed in our experiments lower polarization resistance of electrodes with increased porosity can be explained by the easier diffusion of gas into the electrode, which prevents the oxygen concentration from falling too low. The effect of improving the cathode's operation is less pronounced at lower temperatures because the direct current flowing through the electrode is lower and hence the decrease in oxygen concentration is not so great.

The dependency of polarization resistance on oxygen partial pressure is depicted in Fig. 5. The improvement of electrode properties is denoted in the whole examined concentration range, however, at the lowest concentration, the improvement is not so big. In the case of such small oxygen partial pressure, the amount of oxygen that can reach the deeper layer of the cathode is effectively very low.

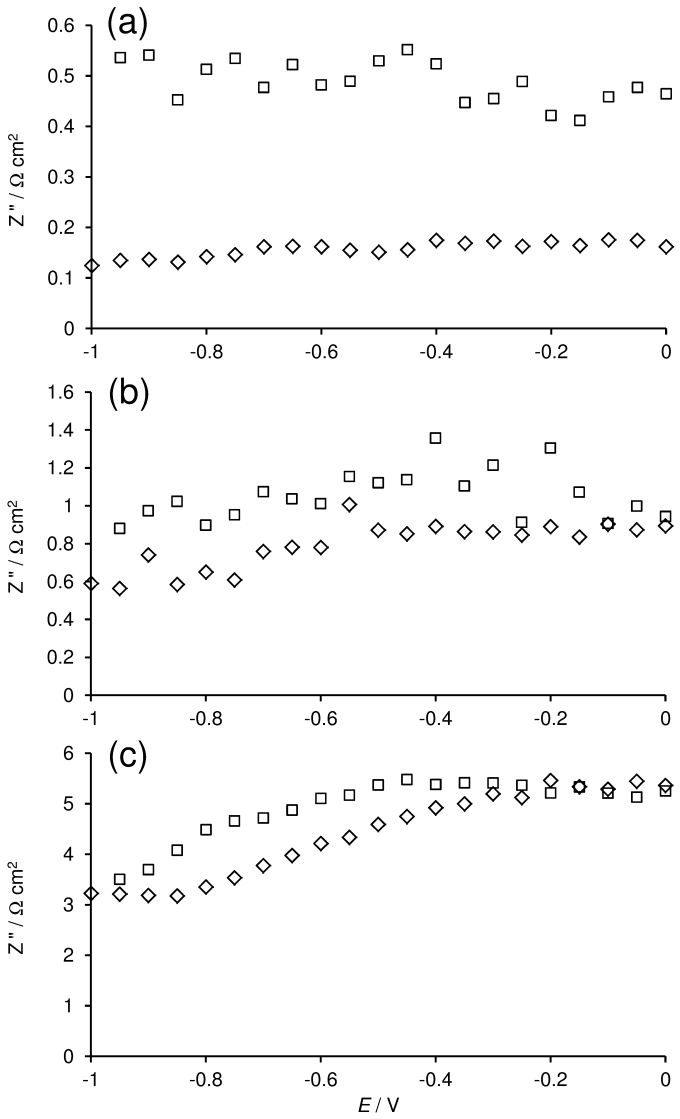

Fig. 4. Polarization resistance of LSCF (squares) and LSCF-PS (diamonds) electrodes measured versus applied potential in synthetic air (20% of oxygen in argon) at: (a) 800; (b) 700; (c) 600°C

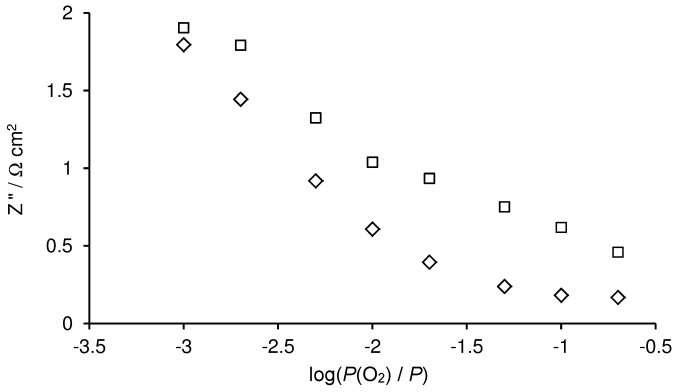

Fig. 5. Polarization resistance of LSCF (squares) and LSCF-PS (diamonds) electrodes measured versus oxygen partial pressure at 800°C

Composite LSCF-YFC cathodes reveal worse performance than pure LSCF ones. The polarization resistance of LSCF-YFC and LSCF-YFC-PS electrodes versus oxygen partial pressure are compared in Fig. 6. Both cathodes reveal greater R_p than similar LSCF and LSCF-PS cathodes, respectively, although the effect of additional porosity from added polystyrene beads in the LSCF-YFC composite electrode is higher than in the LSCF electrode.

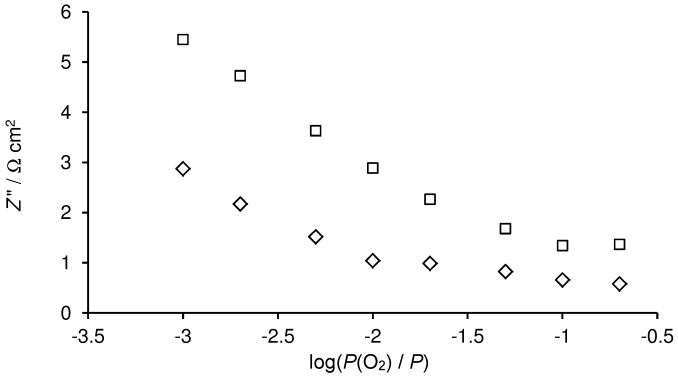

Fig. 6. Polarization resistance of LSCF-YFC (squares) and LSCF-YFC-PS (diamonds) electrodes measured versus oxygen partial pressure at 800°C

4. Conclusions

The effect of addition YFC powder and 6 μm polystyrene beads to electrode ink were examined. The performance of cathodes was evaluated by the measurements of polarization resistance. The cathodes with lower polarization resistance are better because they generate lower energy losses in the cell.

The addition of YFC did not improve electrode performance. The LSFC-YFC and LSCF-YFC-PS cathodes revealed much higher polarization resistance than LSCF and LSCF-PS electrodes, respectively, in the whole examined concentration range.

The addition of polystyrene balls to LSCF and LSCF-YFC cathode inks facilitates gas diffusion in the obtained electrodes of enhanced porosity. These electrodes reveal lower polarization resistances than similar ones without additional porosity. The biggest improvement in performance caused by the additional porosity was achieved at the LSCF electrode at 800°C.

Acknowledgments

This research was funded by the statutory research fund of ICSC PAS. M. Krzan and M. Mosiałek acknowledge also the support of the National Science Centre of Poland research project (grant no. 2016/21/B/ST8/02107).

REFERENCES

[1] K. Hemmes, Fuel Cells, in R.E. White, B.E Conway, C. Vayenas (Eds.), Modern Aspects of Electrochemistry, Springer Vol. **37**, Ch. 4 131-251 (2004). DOI:10.1007/978-1-4419-9027-3_4

[2] S.P.S. Badwal, K. Foger, Ceram. Int. **22**, 257-265 (1996). DOI:10.1016/0272-8842(95)00101-8

[3] A. Jun, S. Yoo, O.-H. Gwon, J. Shin, G. Kim, Electrochim. Acta **89**, 372-376 (2013). DOI:10.1016/j.electacta.2012.11.002

[4] E. Bucher, W. Sitte, G.B. Caraman, V.A. Cherepanov, T.V. Aksenova, M.V. Ananyev, Solid State Ionics **177**, 3109-3115 (2006). DOI:10.1016/j.ssi.2006.07.062

[5] H.J. Hwang, J.-W. Moon, S. Lee, E.A. Lee, J. Power Sources **145**, 243-248 (2005). DOI:10.1016/j.jpowsour.2005.02.063

[6] M. Mosiałek, M. Dudek, J. Wojewoda-Budka, Arch. Metall. Mater. **58**, 275-281 (2013). DOI: 10.2478/v10172-012-0185-2

[7] M. Sahibzada, S.J. Benson, R.A. Rudkin, J.A. Kilner, Solid State Ionics **113-115**, 285-290 (1998). DOI:10.1016/S0167-2738(98)00294-X

[8] J. Chen, F. Liang, B. Chi, J. Pu, S.P. Jiang, L. Jian, J. Power Sources **194**, 275-280 (2009). DOI:10.1016/j.jpowsour.2009.04.041

[9] Z. Liu, M. Liu, L. Yang, M. Liu, J. Ener. Chem. **22**, 555-559 (2013). DOI:10.1016/S2095-4956(13)60072-8

[10] X. Zhu, D. Ding, Y. Li, Z. Lü, W. Su, L. Zhen, Int. J. Hydrogen Energ. **38**, 5375-5382 (2013). DOI:10.1016/j.ijhydene.2013.02.091

[11] S. Lee, N. Miller, M. Staruch, K. Gerdes, M. Jain, A. Manivannan, Electrochim. Acta **56**, 9904-9909 (2011). DOI:10.1016/j.electacta.2011.08.060

[12] X. Lou, S. Wang, Z. Liu, L. Yang, M. Liu, Solid State Ionics **180**, 1285-1289 (2009). DOI:10.1016/j.ssi.2009.06.014

[13] J. Cui, J. Wang, W. Fan, Y. Wan, X. Zhang, G. Li, K. Wu, Y. Cheng, J. Zhou, Int. J. Hydrogen Energ. **42**, 20164-20175 (2017). DOI:10.1016/j.ijhydene.2017.05.109

[14] S.B. Adler, J.A. Lane, B.C.H. Steele, J. Electrochem. Soc. **143**, 3554-3564 , (1996). DOI:10.1149/1.1837252

[15] X.J. Chen, S.H. Chan, K.A. Khor, Electrochim. Acta **49**, 1851-1861 (2004). DOI:10.1016/j.electacta.2003.12.015

[16] Anil V. Virkar, Jong Chen, Cameron W. Tanner, Jai-Woh Kim, Solid State Ionics **131**, 189-198 (2000). DOI:10.1016/S0167-2738(00)00633-0

[17] M. Mosiałek, M. Przybyła, M. Tatko, P. Nowak, M. Dudek, Arch. Metall. Mater. **58**, 1337-1340 (2013). DOI:10.2478/amm-2013-0170

[18] M. Mosiałek, A. Michna, M. Dziubaniuk, E. Bielańska, A. Kežionis; T. Šalkus, E. Kazakevičius, B. Bożek, A. Krawczyk, J. Wyrwa, A. F Orliukas, Electrochim. Acta **282**, 427-436 (2018). DOI:10.1016/j.electacta.2018.06.063

[19] ICDD PDF-4+ 2015 01-084-8433. Database, edited by Dr. Soorya Kabekkodu, International Centre for Diffraction Data, Newtown Square, PA, USA. http://www.icdd.com/

[20] M. Mosiałek, M. Dudek, A. Michna, M. Tatko, A. Kędra, M. Zimowska, J. Solid State Electr. **18**, 3011-3021 (2014). DOI:10.1007/s10008-014-2457-4

[21] M. Mosiałek, M. Dudek, P. Nowak, R.P. Socha, G. Mordarski, E. Bielańska, Electrochim. Acta **104**, 474-480 (2013). DOI: 10.1016/j.electacta.2013.01.117

[22] E.P. Murray, M.J. Sever, S.A. Barnett, Solid State Ionics **148**, 27-34 (2002). DOI: 10.1016/S0167-2738(02)00102-9